www.czasopisma.pan.pl PAN POLSKA AKADEMIA NAUK www.journals.pan.pl

PAN ARCHIVES OF ACOUSTICS
Vol. 40, No. 2, pp. 169–181 (2015)

DOI: 10.1515/aoa-2015-0019

Dynamic Properties of Concrete Composite Panels under Eccentric Compression Loading Tests

Max de Castro MAGALHAES, Roberto M. da SILVA

DEES – Department of Structural Engineering, Federal University of Minas Gerais
Av. Antonio Carlos, 6627, Campus Pampulha, Belo Horizonte 31270901, Brazil; e-mail: maxdcm@gmail.com

(*received October 24, 2014; accepted December 7, 2014*)

The main aim of this paper is to examine the variability of some dynamic properties of concrete composite panels to in-plane eccentric compression loads via static and dynamic impact testing. First, experimental tests were performed in order to obtain the dynamic and static properties of concrete composite panels. In-plane eccentric loads were statically applied to a couple of panels in ten uniform steps. For each step, dynamic impact testing was performed and the modal damping, peak amplitude and natural frequencies obtained. Second, a 'hybrid' model, based on the concepts of modal analysis and the Finite Element Method, was developed in order to obtain the natural frequencies and corresponding normal modes of the composite panels within the frequency range 0–200 Hz. For this model, an initial warp of the panel middle surface was incorporated into the formulation in order to represent the applied flexural moment provoked by the eccentric in-plane loads. The accuracy of the 'hybrid' model was verified by comparison with the experimental results. Third, comparison is made between predictions (using on the 'hybrid' model) and experimental results.

Keywords: dynamic analysis, composite panels, in-plane loading, pre-stressed panels.

1. Introduction

The influence of in-plane loads on the dynamic behavior of plates has been studied for several years (Mamou-Mani *et al.*, 2007; Ilanko, Tillman, 1985; Kielb, Han, 1980). Many researches have presented the results of investigations into the reasons for the observed discrepancies. Measurements were made on rectangular plates to obtain initial geometrical imperfection profiles. It was assumed that the plates were free of residual stress. The plates were loaded axially in-plane. The stress distribution and deflection profiles at particular load values were measured together with the corresponding natural frequencies. It was seen that the vibration response of practical in-plane loaded plates can differ significantly from the response predicted theoretically on the basis of a uniform in-plane stress distribution. It was shown that this difference was due, at least in part, to the redistribution of in-plane stress that occurred in practical plates due to the growth of initial geometrical imperfections with increasing applied load.

Kang and Shim (2004) presented an exact solution procedure for the free vibration analysis of rectangular plates having two opposite edges simply supported that were subjected to linearly varying normal stresses causing pure in-plane moments.

Non-linear equations of large amplitude vibrations have been derived for a laminated plate in a general state o non-uniform initial stress (Chen *et al.*, 2002). The effects of transverse shear strain and rotary inertia were included. In this paper the frequency response showed not only sensitive to the vibration amplitude but also to an arbitrary initial state of stresses. The linear natural frequencies were calculated by neglecting the non-linear terms on the differential equations. It was observed that the effect of non-linearity increased when the initial stress was compressive. In other words, the compressive initial stress produced a hardening effect on the frequency ratio (non-linear frequency to linear frequency). Therefore, the ratio of frequency (non-linear frequency to linear frequency) increased as the compression loads increased.

The basis of the method presented by (Hilmerson *et al.*, 2008) is that the audible impact response from a cracked component sounds different than that of a non-cracked component. From each set of data, the natural frequency, peak magnitude and damping ratio were extracted for each of the four dominant modes.

Experimental tests were carried out to study the strength and behaviour of Ordinary Portland Concrete (OPC) and Geopolymer Concrete (GPC) panel panels (Ganesan *et al.*, 2013). A total of 20 panel panels were tested under uniformly distributed axial load in one-way in-plane action. The main variables considered in this study were slenderness ratio (SR) and aspect ratio (AR) of the panels. The equations available in the literature for predicting the ultimate load of RC (Reinforced Concrete) panel panels were found to be conservative and a new method was proposed to predict the ultimate load of GPC panel panels.

In Ramachandra and Panda (2012) buckling and dynamic instability of composite plates subjected to dynamic loads were investigated. It is seen that the instability regions depends on the in-plane load variation. The boundary conditions of the plate had an influence on the dynamic instability regions.

A study of the buckling behaviour of masonry panels subjected to vertical loading was investigated by Sandoval and Roca (2012). The purpose was to determine the effects of the slenderness ratio, the eccentricity of applied load, the stiffness of the panel and the tensile strength of the unit-mortar interface on the load bearing capacity of masonry panels. It was observed that the slenderness and the flexibility of the panel had some influence on the strength capacity of the panels.

As far as the authors are aware, this paper appears to be the only experimental and numerical study to date on the relationship between natural frequency and in-plane compressive load for composite light concrete panels.

2. Methodology

Firstly, some of the material properties of light concrete panels considered herein were obtained from the literature, others obtained from experimental measurements. The density of each concrete panel was equal to 611 kg/m^3. This value was found in the literature. Alternatively, static and dynamic tests were performed in order to obtain the Young's Modulus E_L and the total loss factor η respectively.

Secondly, a 'hybrid' theoretical model was developed and implemented in order to simulate the effect of in-plane eccentric loads on the natural frequencies of isotropic thin plates. The physical and mechanical properties used on the simulations were measured (e.g. η and E_L) and obtained in the literature. The 'hybrid' model was based on the concepts of modal analysis and the Finite Element Method.

Thirdly, experimental tests were performed on a couple of light concrete panels in order to validate the 'hybrid' model. The tests were made using impact testing. Frequency response functions (FRFs) were recorded and the natural frequencies extracted and compared to those obtained using the 'hybrid' model.

2.1. Experimental tests

Each panel sample was built using three concrete panels bounded together around a particular edge using polyurethane foam adhesive (see Fig. 1). This did not provide ideal tied edges, as it was dependent on

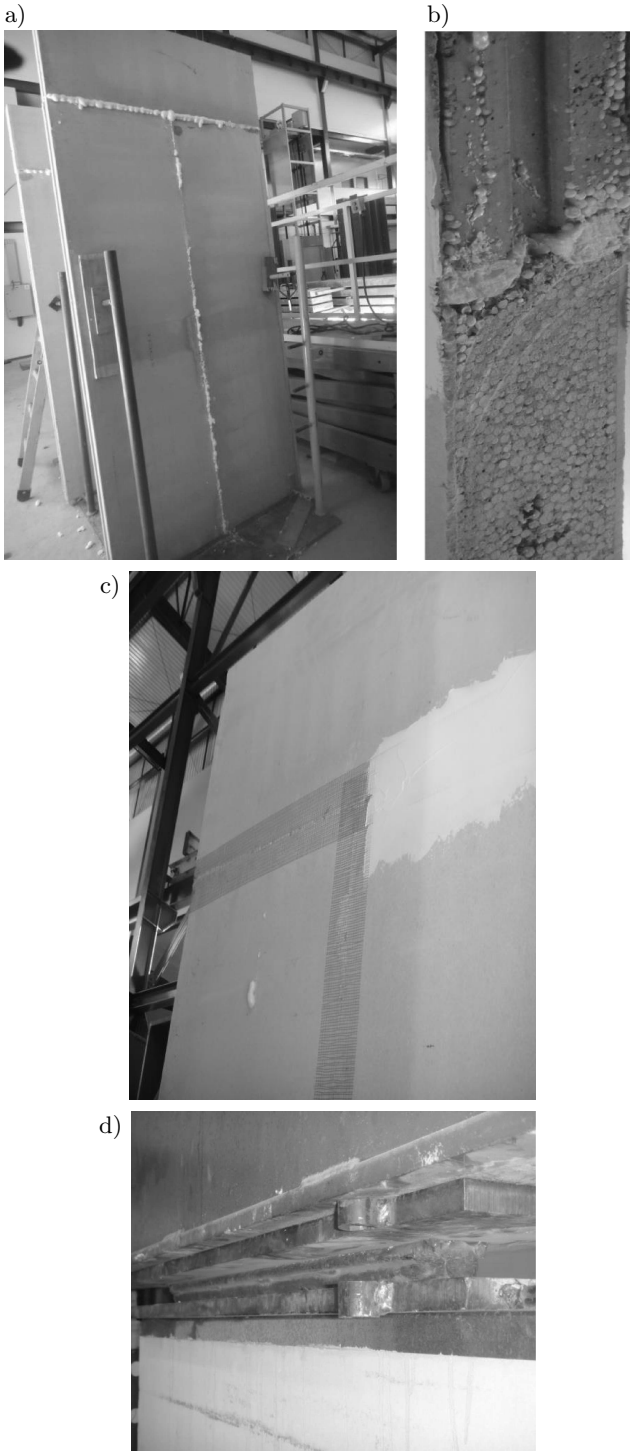

Fig. 1. Photographs of the production of a building panel sample using concrete panels; a) concrete panels bounded by polyurethane foam; b) detail of a joint between two concrete panels; c) panel surface preparation using fabric net and gypsum; d) pinned top edge of the panel.

the stiffness and strength of the adhesive. However, it did provide a reasonable constraint on the flexural displacement. As mentioned previously, experimental tests were performed in order to obtain E_L and η and two samples (see Fig. 1). Experimental tests were made on concrete panels (122×272×9 cm) simply-supported along the top and bottom edges (see Fig. 2). It is seen that the boundary conditions along the lateral panel edges were free. A set of two panels was used in this study.

a)

b)

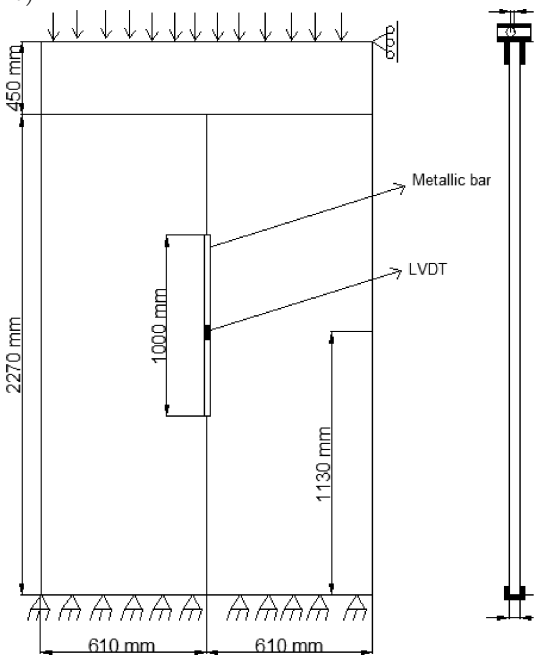

Fig. 2. Set-up of the apparatus used on the static experimental tests; a) photograph of the experimental set-up for the static compression test; b) schematic representation for the compression test.

Dynamic and static tests were made on each specimen. The tests were made at the Structural Engineering Research Laboratory (LAEES). Each panel had the cross-section area equal to 122×9 cm. The concrete panels were tested in the vertical position in a compression testing machine of 200 tons capacity. Pinned end condition was provided at the both supporting ends and uniformly distributed load along panel thickness h_w was applied at a large eccentricity of 30 mm. This value was greater than the central region limit $h_w/6 = 15$ mm. Thus, the central region concept defined on the theory of material strength was used herein in order to reflect possible eccentric load in practice.

Figures 2a and 2b below show the photograph and schematic diagram of the static test set up. Vertical alignment of the panels was ensured by a plumb-bob and a levelling ruler was used to ensure the proper levelling of the panels. The loading was gradually increased in stages up to failure. It was applied on the panels by pressing a rigid I-section steel beam on the top edge of them using a hydraulic-jack. Although the loading steps were applied manually, the rate of loading could be estimated and was equal to 2.0 ton per minute. At each stage, lateral deformation at mid-height point was measured using LVDT sensors. The experimental ultimate loads were also recorded. A statistical model was considered using the least-square fitting method. The slope of the tangent drawn to the stress-strain curve at a given stress value was calculated and the tangent modulus E_L obtained.

The damping η is known as total loss factor. The values of damping η are sometimes termed structural damping, to identify that the damping is dependent on both the damping inherent in the material and that which comes from other mechanisms including dissipation losses at the boundary which might be significant. In other words, the total loss factor is equal to the sum of the internal loss factor of the material, the coupling loss factor to the adjacent structures and the radiation loss factor to the surrounding media (Fahy, 1985).

The apparatus set-up used on the dynamic experimental tests is shown in Fig. 3 below.

First, the impulse responses were obtained using the impact testing procedure described as follows. On impacting the panel sample by an instrumented hammer, the analyzer was triggered and started recording the response signal at the receiving point, where accelerometers were attached and connected to the acquisition equipment (National Instruments data acquisition module type NI-9233). The input signal was filtered by conveniently configuring the channel parameters.

a)

b)

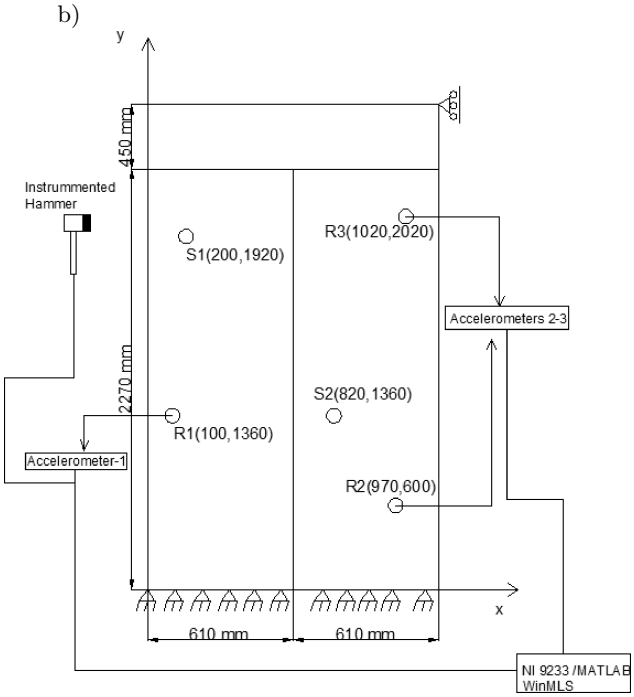

Fig. 3. Set-up of the apparatus used on the dynamic tests; a) photograph of the experimental set-up for the dynamic test; b) schematic representation.

The signal $s(t)$ received at the receiving point is given by (Meirovitch, 1967; Cremer *et al.*, 1988)

$$s(t) = \int_{-\infty}^{t} f(\tau)h(t-\tau)\,\mathrm{d}\tau, \tag{1}$$

where $f(t)$ is input excitation force and $h(t)$ is the impulse response of the system. For an impulse at time t_i one has

$$f(\tau) = F_o\delta(\tau - t_i), \quad \text{then} \quad s(t) = F_o h(t - t_i), \tag{2}$$

where F_o is the input excitation force amplitude.

Second, the aim was to measure the natural frequencies of the concrete panel using the frequency response functions (FRFs) defined by (Sandoval, Roca, 2012)

$$H_{ji} = \frac{S_{ij}}{S_{ii}} \ [\mathrm{m\ s^{-2}/N}], \tag{3}$$

where S_{ij} and S_{ii} are the cross-spectral density function (for a force applied at point i and the corresponding velocity measured at point j) and the autospectral density function (for a force applied at point i and the corresponding velocity also measured at point i) respectively.

These functions were obtained via Fourier transforms of the measured quantities. These functions are also named mobilities or velocity transfer functions. A frequency range of 0–200 Hz was considered on the experimental tests. The vibration source was a plastic-headed hammer. It was used to hit the concrete panel at different locations (in order to obtain the H_{ji}) over a period of 8 seconds.

The point mobility of the system was obtained by measuring the impact force and the acceleration which was later integrated in order to obtain the velocity. The average transverse vibration level of each panel was measured for a 'no in-plane loading' condition and for ten distinct in-plane load steps. The velocities were determined by integrating the accelerations at every frequency line. The FRF 'sweeps' using the instrumented hammer resulted in 6 FRFs which were acquired over three response and two excitation test points as a reference (see Fig. 3).

Alternatively, a simple technique used in (Cremer *et al.*, 1988) helps the selection of frequencies which may correspond to the modes of vibration. Thus, another simple parameter named Mode Indicator Function (MIF) and denoted as $|H_{j,\mathrm{sum}}(\omega)|$ can be defined. It is the sum of the moduli of all measured FRFs. It is given by (Pavic, Reynolds, 2003):

$$|H_{j,\mathrm{sum}}(\omega)| = \sum_i H_{ji}(\omega). \tag{4}$$

Then, the peaks corresponding to the coupled natural frequencies were identified on each PSD curve.

Third, once the resonance frequencies f_n were identified from the measured impulse responses, the corresponding half-value bandwidths b could be determined. The total loss factor was calculated as

$$\eta = \frac{b}{f_n}. \tag{5}$$

Finally, the data from the measurements were analysed in order to assess the variation of natural frequency, peak magnitude, and mode bandwidth with eccentric in-plane load values. The findings were consistent with the expected dynamic behaviour of concrete panels under in-plane eccentric loads.

2.2. Numerical simulations

Numerical simulations are presented for a simply-supported panel under eccentric in-plane loads, commonly found on the process of building construction. A FE model was considered in order to find the corresponding normal modes for specific loading conditions. Ten loading steps were considered for the in-plane loaded panels. A frequency range of 0–200 Hz was considered on the numerical simulations.

The analyses were performed on two distinct stages as follow.

Firstly, the commercial FE (Finite Element) software, namely ABAQUS (ABAQUS/CAE – User's Manual v6.7), was used in order to obtain the mode shapes $\phi_p(z,y)$ (and their corresponding natural frequencies) for the 'no in-plane load case', and consequently to validate the FE model against its analytical counterpart. A convergence criteria based on energy was used. A tolerance value of 10^{-3} was considered.

Secondly, the equation of motion for rectangular thin plates with two simply-supported edges was derived considering the combined action of uniform lateral load and uniform tension.

Finally, a modal model based on the equations of motion was developed and implemented in MATLAB in order to simulate the effect of in-plane eccentric loads on the natural frequencies of isotropic thin plates.

The concrete panels considered herein had a bending stiffness equal to B' and were pre-stressed with an eccentric compression stress. In other words, the panel did experience bending under the action of in-plane compression forces. This is equivalent to the effect of a fictitious initial curvature on the deflection.

In this study the applied flexural moment, which was provoked by the eccentric in-plane loads, was represented by some initial warp of the panel middle surface. This procedure is justifiable if at any point of the panel there was an initial deflection w_o which was small in comparison with the thickness of the plate (Timoshenko *et al.*, 1959). If such a panel is submitted to the action of transverse loads, additional deflection w_1 will be produced and applying the principle of superposition, the total deflection at any point will be $w_1 + w_o$. Hence, for the case of an initial curvature, the equation of motion is given by Timoshenko *et al.* (1959) and Blevins (1995)

$$B'\nabla^4 w_1 - T'_y \frac{\partial^2}{\partial y^2}(w_o + w_1) + c\frac{\partial w_1}{\partial t} + m''\frac{\partial^2 w_1}{\partial^2 t} = f(xy,t), \quad (6)_1$$

$$w_o = \frac{-M_o y^2 + \nu M_o x^2}{2B'(1-\nu^2)}, \qquad w_1 = \overline{w}_1 e^{j(\omega t - k_x x - k_y y)}, \quad (6)_2$$

where T'_y is the normal in-plane load per unit length of edge (in the y direction), c is the viscous damping coefficient per unit area of the plate, m'' is the mass per unit area of the plate, $\overline{w}_1$ is the complex amplitude of the panel deflection w_1 into the air, ω is the frequency of the applied harmonic force, k_x and k_y are structural wavenumber components in the x and y direction respectively, ν is the Poisson's ratio, $f(xy,t)$ is the externally applied harmonic point force excitation per unit area, M_o [N m/m] is the applied moment per unit width in the panel edge x.

The thickness of each panel sample was 90 mm. The basis of the criterion for 'thinness' adopted was $k_b h_p < 1$, where k_b is the free structural wave number and h_p is the panel thickness. Each panel was assumed to be free and simply-supported mounted in the x and y direction considering a plane of the Cartesian coordinate system. A typical basis function that might be used as a modal expansion for the panel deflection must ensure a vanishing normal displacement on the contour of the panel in the y direction and a unit normal displacement in the x direction. It satisfies the free and simply supported boundary conditions and *in vacuo*, is given by

$$\phi_p(x,y) = \cos(k_x x)\sin(k_y y), \qquad k_x = \frac{r\pi}{L_x}, \qquad k_y = \frac{s\pi}{L_y}. \quad (7)$$

L_x is the width of the panel, L_y is the length of the panel, and r, s represent the panel mode numbers.

The response (normal displacement to the plate surface) of the plate to a harmonic point force excitation f_o at position $(x_o y_o)$ and at frequency ω is given by

$$w_1(z,y,\omega) = \sum_{p=1}^{P} w_p \phi_p, \qquad F_p = \int_S f(x,y)\phi_p(x,y)\,\mathrm{d}s, \quad (8)$$

where P is the total number of structural modes considered.

Then, Eq. $(8)_1$ may be an expression for the concrete panel displacement in terms of a summation of its assumed-modes. The modal response (displacement) of

panel was represented by w_p. Substituting Eqs. $(8)_1$ and $(8)_2$ into Eq. $(6)_1$, multiplying by ϕ_p and integrating over the partition surface yields the modal equations

$$\left\{-\omega^2 + j\omega\beta_p + \omega_p^2 + \frac{T'_y}{m''} \cdot \left(k_y^2 + \frac{M_o}{B'(1-\nu^2)}\right)\right\} w_p = \frac{F_p}{\Lambda_p}, \quad (9)$$

where ω is the excitation frequency in radian/s and F_p is the generalized force applied on the concrete panel. The term $j\omega\beta_p w_p$ is added on the left-hand side of Eq. (9) in order to represent the damping of the flexible panel. β_p is the generalized modal damping coefficient, which is given by $\eta_p\omega_p$ for the panel; Λ_p is the modal mass of the structural mode p; ω_p represents the p-th natural frequency of the panel. The value of T'_y in Eq. (9) is negative for compressive loads. The structural modes ϕ_p used herein were obtained from the FE simulations. Alternatively, they might have been calculated using Eqs. $(7)_1$ and $(7)_2$.

The numerical model was validated and used to perform a parametric study involving the variation of applied static loads (flexural moment and compression load) in order to assess the influence of them on the panel dynamic stiffness.

3. Results and discussion

As mentioned previously, the determination of the concrete panel properties was obtained experimentally. The longitudinal Young's modulus E_L was obtained by a static experimental test. Figures 4 and 5 below show the slope of the straight line in a stress-strain curve. The results presented are shown for two panel samples. Figure 4 below shows the variation of normal stress with strain obtained via experimental test for sample 1. The determination coefficient R^2 found for this model was equal to 0.98. The Young's modulus was determined using the first part of the curve. Its value was equal to 4.5 GPa.

Figure 5 below shows the variation of normal stress with strain obtained via experimental test for sample 2. Likewise, the statistical model presented was obtained via curve fitting. The determination coefficient R^2 found for this model was equal to 0.99. The Young's modulus was determined using the first part of the curve. Its value was equal to 4.9 GPa.

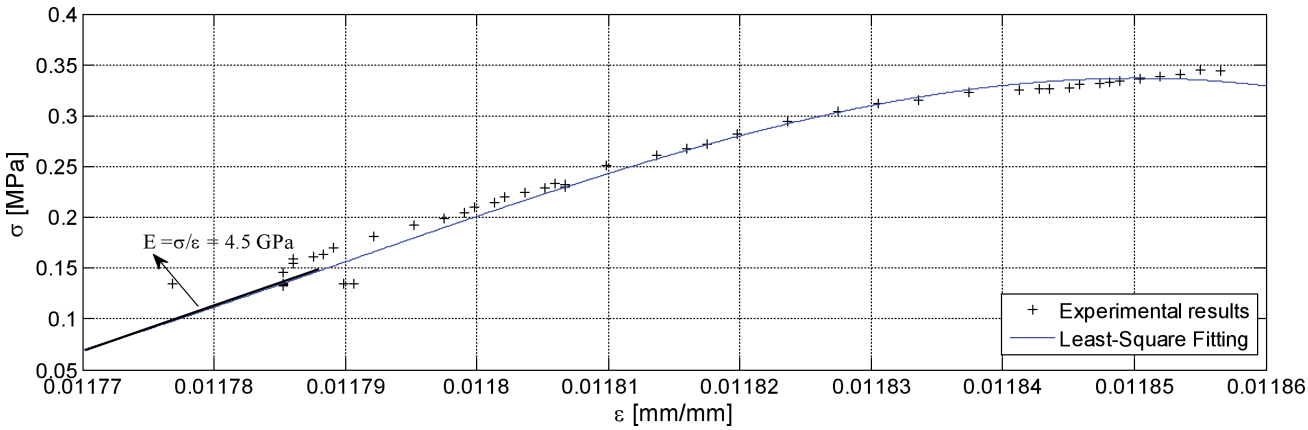

Fig. 4. Variation of normal stress with normal strain for sample 1 subjected to compression loading.

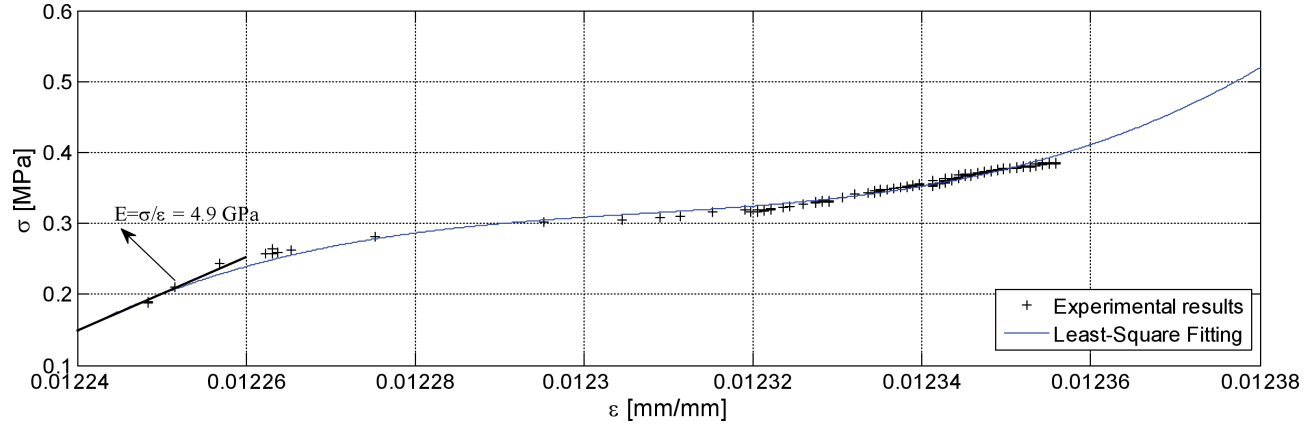

Fig. 5. Variation of normal stress with normal strain for sample 2.

Next, the average loss factors obtained via impact testing are presented on Table 1 below. Table 1 shows the values of η obtained only for the first 3 structural modes. It is due to the high damping values of composite concrete panels considered herein.

Table 1. Total loss factor of the concrete panel.

Vibration Mode Number	η
1	0.22
2	0.1
3	0.07

Afterwards, static loads were applied to the panel. Ten static load steps were considered (see Figs. 6a and 6b).

As mentioned before, the loading steps were applied manually. It is seen on Fig. 6a that each applied load was relaxed after few minutes. The rate of loading could also be estimated and was equal to approximately 2.0 ton per minute. Figure 6b shows the time averaged values of the static load for each step.

Next, impact testing was again performed for each static load step. The first seven load steps led to crack-free panels. Table 2 below shows a comparison between groups of structural natural frequencies obtained experimentally, numerically using the FE model and analytical formula (Blevins, 1995).

Table 2. Comparison between groups of natural frequencies of an unloaded concrete panel obtained experimentally, numerically (using FEM) and analytically.

Number	Mode		
	F_N [Hz] (Measured)	F_N [Hz] (FEM)	F_N [Hz] (Blevins, 1995)
1	13.8	14.6	11.6
2	45.5	45.5	41.1
3	63.5	55.5	46.9
4	95.0	103.4	91.9
5	111.5	123.8	106.4
6	156.0	157.9	159.5
7	183.0	179.1	–
8	225.2	226.0	–

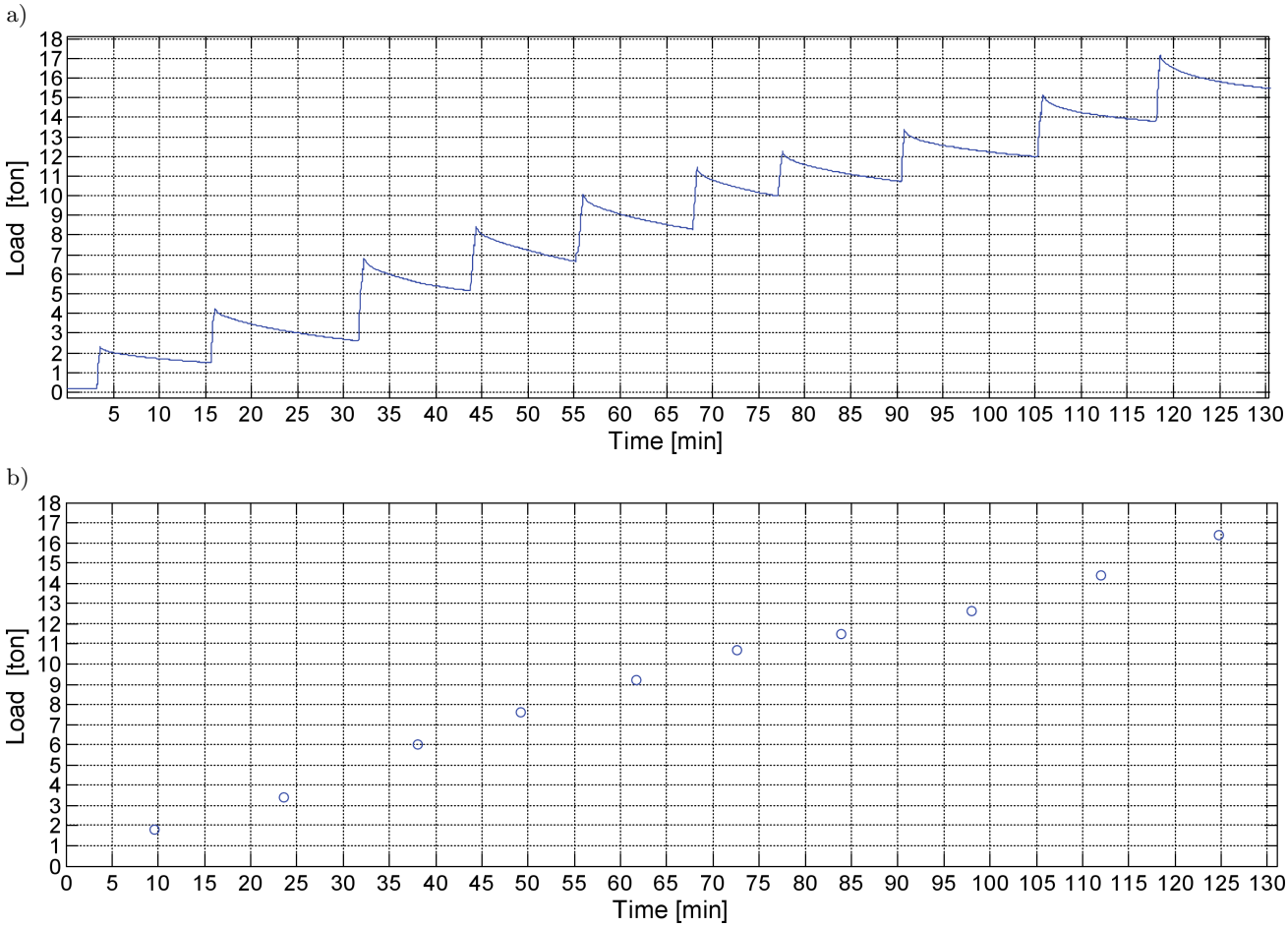

Fig. 6. Variation of applied static loads with time; a) rate of applied static loading, b) mean values of applied static load on each step.

a) $f_1 = 14.6$ Hz (1st mode)

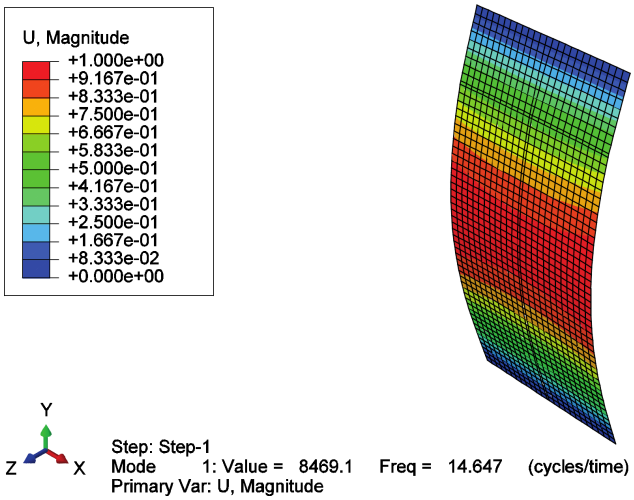

b) $f_2 = 45.5$ Hz (2nd mode)

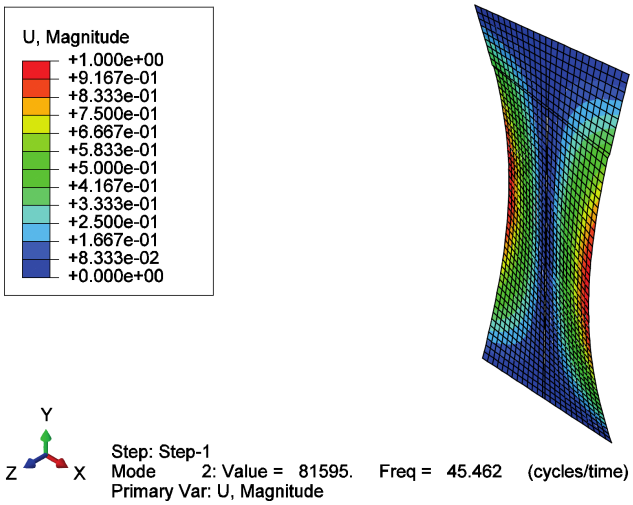

c) $f_3 = 55.5$ Hz (3rd mode)

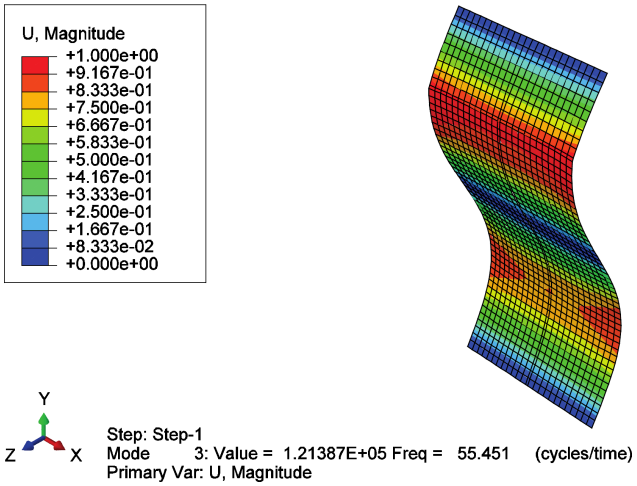

d) $f_4 = 103.4$ Hz (4th mode)

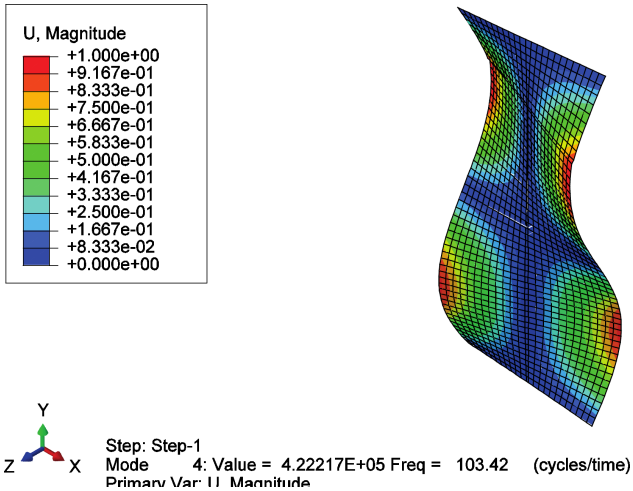

e) $f_5 = 123.8$ Hz (5th mode)

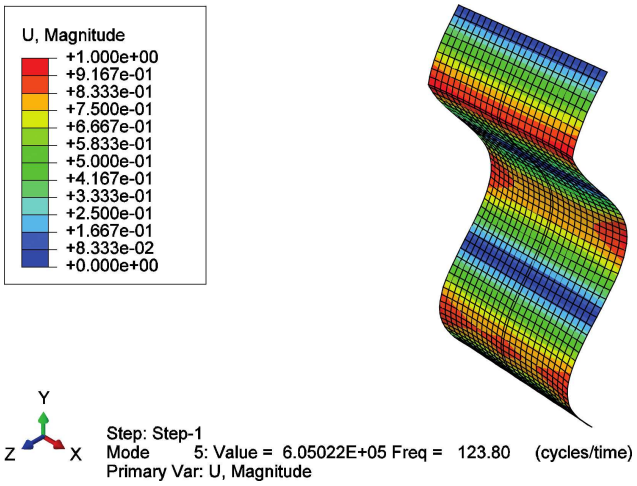

f) $f_6 = 157.9$ Hz (6th mode)

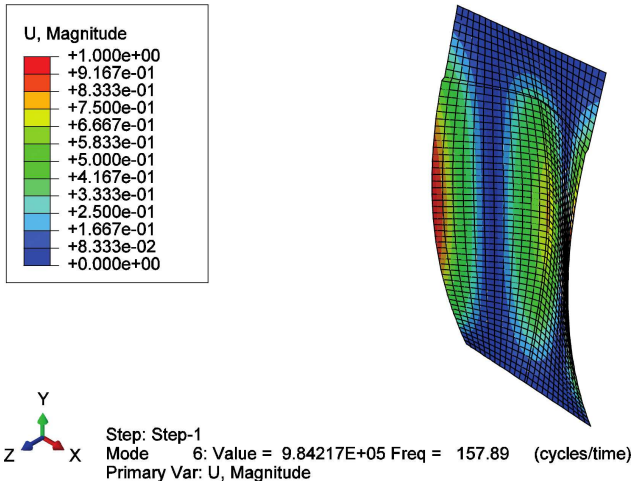

Fig. 7. Set of structural displacement modes for a particular concrete panel sample. It shows the first 6 simply-supported modes. The FE model was statically unloaded.

Table 3 shows that there is a highly significant relationship as the significance value is less than 0.01.

Figure 7 presents the set of structural displacement modes for a concrete panel sample obtained via a FE model. It is shown that the first 6 two-edge simply-supported modes were at frequencies below 160 Hz. All modes in the frequency range 0–200 Hz were considered.

The results on Tables 4 and 5 are consistent with the findings suggesting that the measured and numerical results did not present significant variation. The paired samples statistics for the natural frequencies corresponded to the first 8 (measured and FEM values) and 6 (Blevins' values) modes of the system. Paired samples correlation for the natural frequencies was calculated. They corresponded to the modes of the structural concrete panels. The correlation coefficient varied from 0.992 to 0.996. The results were statistically significant as $p < 0.01$.

Figures 8 and 9 show the relative variation of the natural frequencies with load. It is seen that all investigated modes have their corresponding natural frequencies increased as the in-plane load increases. Besides, Table 6 presents the descriptive statistics for each natural frequency.

Figure 10 shows the relative variation of mode amplitude with load. It is seen that the peak amplitudes do not vary in a predictable pattern. Table 7 presents the descriptive statistics for each peak amplitude.

Table 3. Correlation between groups of natural frequencies of a concrete panel.

		Measured	FE	Blevins
Measured	Pearson Correlation	1	.996**	.994**
	Sig. (2-tailed)		.000	.000
	N	8	8	6
FEM	Pearson Correlation	.996**	1	.992**
	Sig. (2-tailed)	.000		.000
	N	8	8	6
Blevins	Pearson Correlation	.994**	.992**	1
	Sig. (2-tailed)	.000	.000	
	N	6	6	6

** Correlation is significant at the 0.01 level (2-tailed).

Table 4. The paired samples statistics for the natural frequencies of the unloaded concrete panel corresponded to the first 8 (FEM and measured) and 6 (Blevins's results) modes of the system. Correlation between groups of natural frequencies of a concrete panel.

	N	Minimum	Maximum	Mean	Std. Deviation	Skewness		Kurtosis	
Measured	8	13.8	226.0	111.788	72.3875	0.295	0.752	−0.945	1.481
FEM	8	14.6	225.2	113.125	72.4350	0.164	0.752	−1.077	1.481
Blevins	6	11.60	159.50	76.2333	53.59305	0.526	0.845	−0.423	1.741
Valid N (listwise)	6								

Table 5. The paired samples test for the natural frequencies corresponded to the first 7 modes of the system.

		Paired Differences					*t*	df	Sig. (2-tailed)
		Mean	Std. Deviation	Std. Error Mean	95% Confidence Interval of the Difference				
					Lower	Upper			
Pair 1	Measured – FEM	−1.3375	6.4547	2.2821	−6.7337	4.0587	−0.586	7	0.576
Pair 2	Measured – Blevins	4.65000	6.60144	2.69503	−2.27779	11.57779	1.725	5	0.145
Pair 3	FEM – Blevins	7.21667	6.74401	2.75323	0.13926	14.29407	2.621	5	0.047

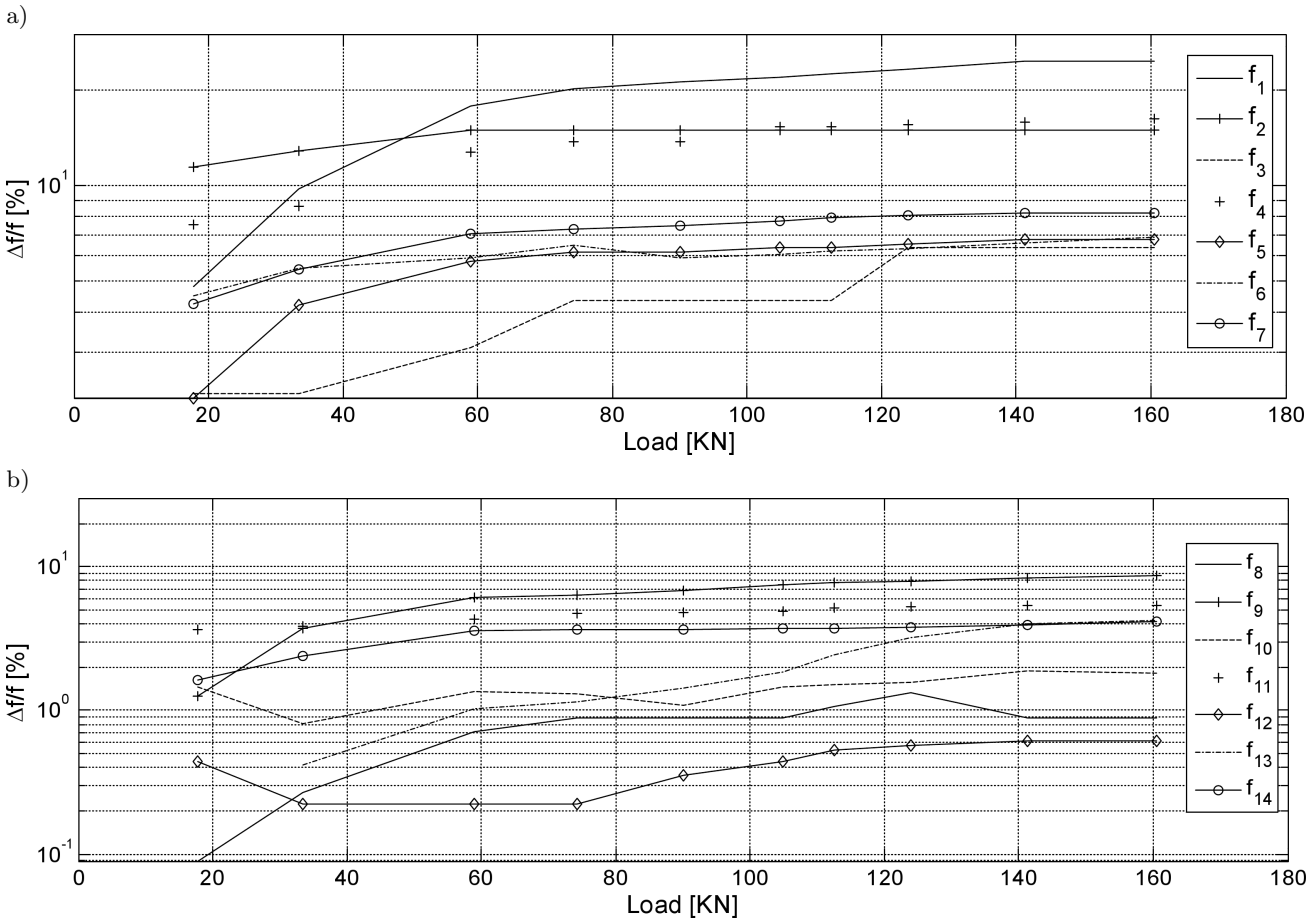

Fig. 8. Relative variation of eigenfrequencies with load; a) eigenvalues $f_1 - f_7$; b) eigen values $f_8 - f_{14}$.

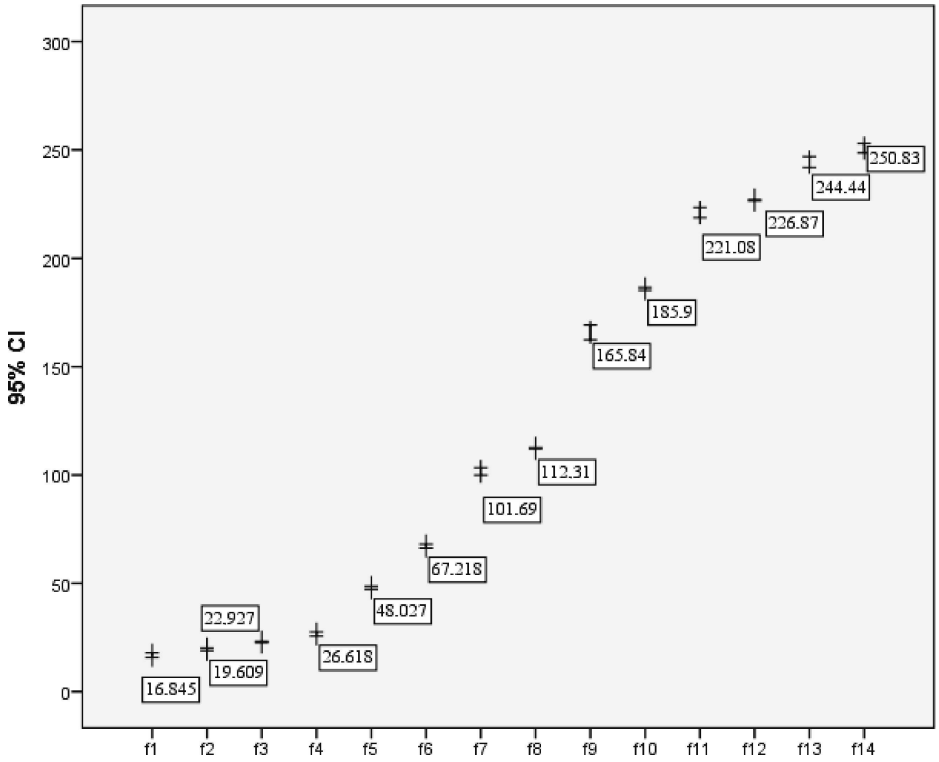

Fig. 9. Confidence interval (95%) of averaged natural frequencies obtained via impact loading. The mean values of all loading steps are also showed.

Table 6. Descriptive statistics for each natural frequency.

	N	Minimum	Maximum	Mean	Std. Deviation	Variance	Skewness		Kurtosis	
	Statistic	Statistic	Statistic	Statistic	Statistic	Statistic	Statistic	Std. Error	Statistic	Std. Error
f_1	11	13.80	18.30	16.8455	1.58137	2.501	−1.090	0.661	−0.229	1.279
f_2	11	17.00	20.00	19.6091	0.90604	0.821	−2.852	0.661	8.499	1.279
f_3	11	22.00	23.50	22.9273	0.47768	0.228	−0.448	0.661	−0.182	1.279
f_4	11	23.30	27.80	26.6182	1.40201	1.966	−1.572	0.661	2.113	1.279
f_5	11	45.50	48.80	48.0273	1.08728	1.182	−1.713	0.661	2.071	1.279
f_6	11	63.50	68.20	67.2182	1.31363	1.726	−2.676	0.661	7.723	1.279
f_7	11	95.00	103.50	101.6909	2.59710	6.745	−2.046	0.661	4.225	1.279
f_8	11	111.50	113.00	112.3091	0.47213	0.223	−0.690	0.661	−0.453	1.279
f9	11	156.00	170.80	165.8364	5.00425	25.043	−1.150	0.661	0.118	1.279
f_{10}	11	183.50	187.00	185.9000	0.97673	0.954	−1.580	0.661	3.171	1.279
f_{11}	11	211.50	223.50	221.0818	3.45625	11.946	−2.472	0.661	6.812	1.279
f_{12}	11	226.00	227.40	226.8727	0.45407	0.206	−0.535	0.661	−0.553	1.279
f_{13}	11	240.00	250.50	244.4364	3.75959	14.135	0.498	0.661	−1.034	1.279
f_{14}	11	243.00	253.50	250.8273	3.22028	10.370	−1.807	0.661	2.789	1.279
Valid N (listwise)	11									

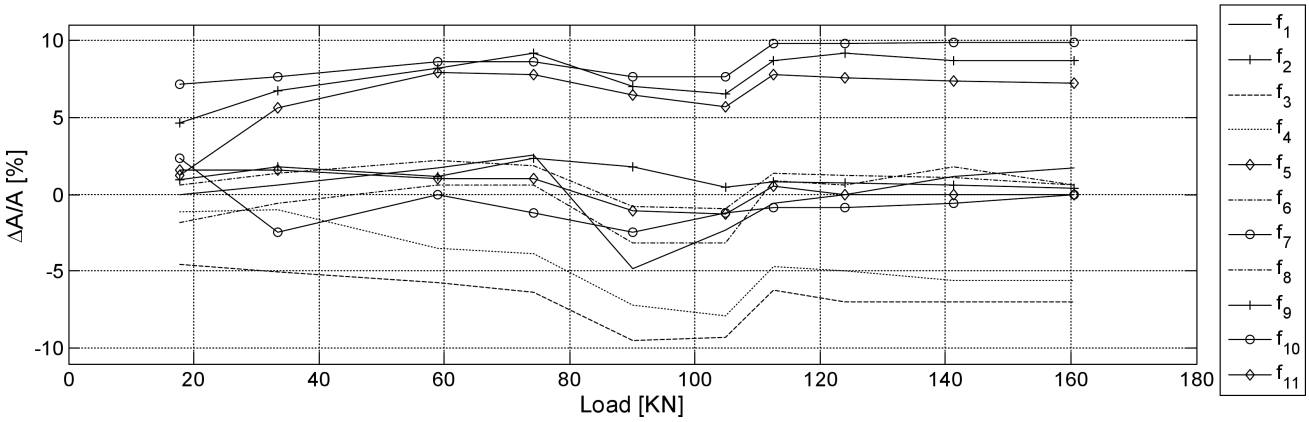

Fig. 10. Relative variation of mode amplitude with load.

Table 7. Descriptive statistics for each peak amplitude.

	N	Minimum	Maximum	Mean	Std. Deviation	Variance	Skewness		Kurtosis	
	Statistic	Statistic	Statistic	Statistic	Statistic	Statistic	Statistic	Std. Error	Statistic	Std. Error
Amplitude1	11	83.00	89.30	87.0273	1.76867	3.128	−1.207	0.661	1.773	1.279
Amplitude2	11	86.30	95.00	92.9000	2.59923	6.756	−1.875	0.661	3.830	1.279
Amplitude3	11	84.00	92.00	86.7182	2.13861	4.574	1.412	0.661	3.521	1.279
Amplitude4	11	82.50	89.00	85.5182	2.10752	4.442	0.356	0.661	−0.846	1.279
Amplitude5	11	93.80	96.50	95.3000	0.90554	0.820	−0.252	0.661	−0.737	1.279
Amplitude6	11	88.20	91.00	89.7000	0.90664	0.822	−0.482	0.661	−0.595	1.279
Amplitude7	11	85.00	94.30	92.3182	2.65323	7.040	−2.376	0.661	6.655	1.279
Amplitude8	11	79.00	83.00	81.2455	1.34266	1.803	−0.837	0.661	−0.508	1.279
Amplitude9	11	83.50	85.50	84.3455	0.60227	0.363	0.665	0.661	−0.263	1.279
Amplitude10	11	81.00	85.00	82.4636	1.09843	1.207	0.950	0.661	2.244	1.279
Amplitude11	11	79.50	86.30	84.5182	2.36170	5.578	−1.568	0.661	1.317	1.279
Valid N (listwise)	11									

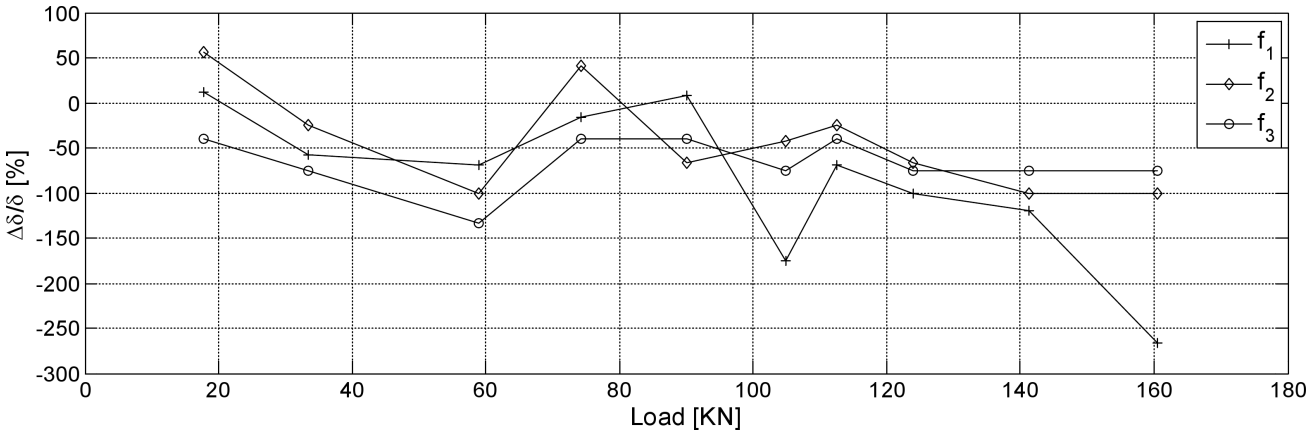

Fig. 11. Relative variation of modal damping with load.

Table 8. Descriptive statistics for each modal damping.

	N	Minimum	Maximum	Mean	Std. Deviation	Variance	Skewness		Kurtosis	
	Statistic	Statistic	Statistic	Statistic	Statistic	Statistic	Statistic	Std. Error	Statistic	Std. Error
Damping1	11	.06	.25	.1500	.06527	.004	.377	.661	−1.227	1.279
Damping2	11	.05	.23	.0909	.05770	.003	1.852	.661	2.845	1.279
Damping3	11	.03	.07	.0455	.01036	.000	1.173	.661	2.623	1.279
Valid N (listwise)	11									

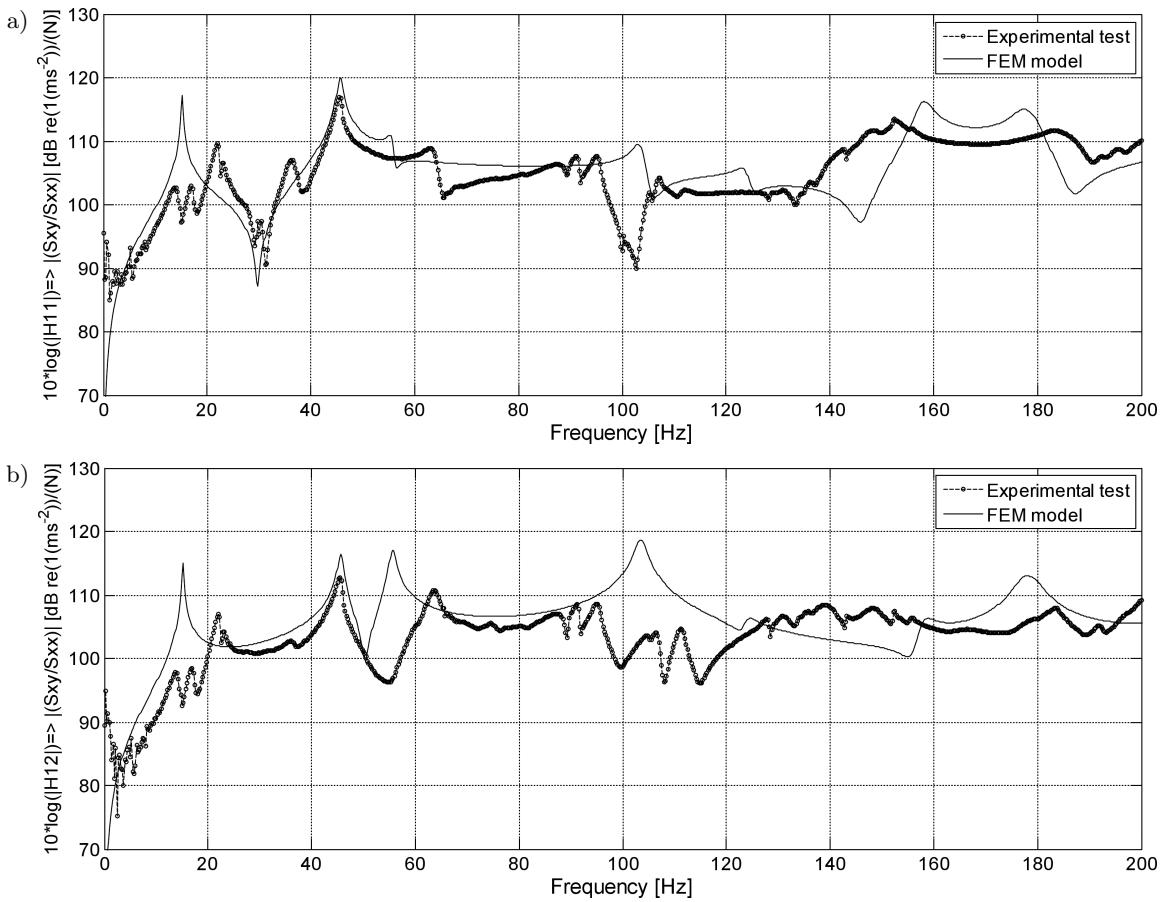

Fig. 12. Variation of the FRFs with frequency for the composite panel: a) H_{11}, b) H_{12}.

Figure 11 shows that the relative variation of the first three modal damping decreases with load. In high frequency ranges, the damping could not be estimated using the half-power bandwidth method due to broadband modes and high modal density. Table 8 shows the descriptive statistics for each modal damping.

Figure 12 shows the variation of the FRFs with frequency (Equation 8) for a simply-supported concrete panel. The results obtained are fairly similar, and consequently provide the validation of the FE model against its experimental counterpart. The structural modes are shown in Fig. 7.

4. Conclusions

The natural frequency of prestressed concrete panels increases as the prestressing force in the load stage increases, but the existing theoretical analysis formulas do not reflect this trend of change. In addition, there are some defects for the existing formulas to adopt uniform modality to calculate the frequencies of linearly distributed external prestressed panels. Using the modified formula to calculate the natural frequency of prestressed panels, one can obtain results which are close to the experimental results. However, the applicability of the formula need to be validated with more experiments. After the panel was loaded, its stiffness was altered substantially. According to the formulation, it depends on the type of loading. Larger pre-stressing force caused a greater axial compressive force, resulting in a decrease in natural frequency. Comparison of the damping factors before and after the load indicated that, unlike the natural frequency, which showed a distinctive tendency, the damping factor shows varied tendencies. The damping factor did not show any significant change. The increases in flexural stiffness and the decreases in damping factor are related. Since the natural frequency increased, it is assumed that the apparent flexural stiffness of the panel increased. Further experiments are needed for higher modes of vibration.

Acknowledgment

Thanks to FAPEMIG (The Research Foundation of Minas Gerais State).

References

1. ABAQUS/CAE – *User's Manual v6.7.*
2. Blevins R.D. (1995), *Formulas for natural frequency and mode shape*, Krieger Publishing Company Press.
3. Chen C.S., Cheng W.S., Chien R.D., Dong J.L. (2002), *Large amplitude vibration of an initially stressed ply laminated plates*, Applied Acoustics, **63**, 939–956.
4. Cremer L., Heckl M., Ungar E.E. (1988), *Structure-borne Sound*, Springer-Verlag, Berlin.
5. Fahy F.J. (1985), *Sound and structural vibration*, Academic Press, U.K.
6. Ganesan N., Indira P.V., Santhakumar A. (2013), *Prediction of ultimate strength of reinforced geopolymer concrete panel panels in one-way action*, Construction and Building Materials, **9**, 1, 91–97.
7. Hilmerson C., Hess D.P., Dallas W., Ostapenko S. (2008), *Crack detection on single-crystalline silicon wafers using impact testing*, Applied Acoustics, 755–760.
8. Ilanko S., Tillman S.C. (1985), *The natural frequencies of in-plane stressed rectangular plates*, Journal of Sound and Vibration, **98**, 25–34.
9. Kang J.H., Shim H.J. (2004), *Exat solutions for the free vibrations of rectangular plates having in-plante moments acting on two opposite simply-supported edges*, Journal of Sound and Vibration, 933–948.
10. Kielb R.E., Han L.S. (1980), *Vibration and buckling of rectangular plates under in-plane hydrostatic loading*, Journal of Sound and Vibration, **70**, 543–555.
11. Mamou-Mani A., Le Moyne S., Frelat J., Besnainou C., Ollivier F. (2007), *Effect of prestresses on natural frequencies of a buckled wooden plate: a numerical and experimental investigation*, Proceedings of the International Conference on Noise and Vibration Engineering (ISMA).
12. Meirovitch L. (1967), *Analytical methods in vibrations*, Macmillan New York.
13. Pavic A., Reynolds P. (2003), *Modal testing and dynamic FE model correlation and updating of a prototype high-strength concrete floor*, Cement and Concrete Composites, **25**, 787–799.
14. Ramachandra L.S., Panda S.K. (2012), *Dynamic instability of composite plates subjected to non-uniform in-plane loads*, Journal of Sound and Vibration, 53–65.
15. Sandoval C., Roca P. (2012), *Study of the influence of different parameters on the buckling behaviour of masonry panels*, Construction and Building Materials, **35**, 1, 888–899.
16. Timosshenko S.P., Woinowsky-Krieger S. (1959), *Theory of plates and Shells*, McGraw-Hill Press.